Ab initio theory of magnetic-field-induced odd-frequency two-band superconductivity in MgB_2

Alex Aperis,* Pablo Maldonado, and Peter M. Oppeneer
Department of Physics and Astronomy, Uppsala University, P.O. Box 516, SE-75120 Uppsala, Sweden
(Received 26 March 2015; published 31 August 2015)

We develop the anisotropic Eliashberg framework for superconductivity in the presence of an applied magnetic field. Using as input the *ab initio* calculated electron and phonon band structures and electron-phonon coupling, we solve self-consistently the anisotropic Eliashberg equations for the archetypal superconductor MgB_2. We find two self-consistent solutions, time-even two-band superconductivity, as well as unconventional time-odd s-wave spin triplet two-band superconductivity emerging with applied field. We provide the full momentum, frequency, and spin-resolved dependence and magnetic field-temperature phase diagrams of the time-even and time-odd superconducting pair amplitudes and predict fingerprints of this novel odd-frequency state in tunneling experiments.

DOI: 10.1103/PhysRevB.92.054516 PACS number(s): 74.20.Rp, 74.20.Pq, 74.25.Dw, 74.55.+v

I. INTRODUCTION

The pair amplitude of the two electrons forming the Cooper pair in a superconductor has to obey the Pauli exclusion principle, which implies that the two-particle amplitude has to be antisymmetric under particle exchange. It is generally assumed that the pair amplitude is symmetric, or even, with respect to the time-argument difference of the two electrons, which leads to the standard classification of Cooper pair wave functions in terms of the remaining symmetry under spatial and spin rotation [1]. It was, however, pointed out by Berezinskii [2] that the antisymmetry of the pair amplitude can be fulfilled equally well when it is odd in time or frequency. Such type of superconductivity cannot be described within Bardeen-Cooper-Schrieffer theory. After odd-frequency superconductivity was first proposed for ^{3}He [2], it has since then been proposed for several materials, including disordered Fermi liquids [3], high-T_c compounds [4], heavy fermions [5], and hydrates [6]. Odd-frequency superconductivity was also predicted to occur at superconductor to ferromagnet or to normal metal interfaces where the spatial symmetry is broken [7–12]. However, in spite of active research and the important ramifications for our understanding of superconductivity, unequivocal observation of this exotic superconducting state remains elusive [13].

Remarkably, it was not until recently that the stability of bulk odd-frequency superconductivity was theoretically established [14,15], thus opening up a window to its experimental detection. Among all potential states, odd-frequency s-wave spin triplet (OST) superconductivity [2] appears as the most robust since it can endure pair breaking by static nonmagnetic impurities [4]. However, in a bulk material, the OST state cannot prevail over the even-frequency counterpart unless an extremely strongly coupled and retarded electron-phonon interaction is at play [16]. Until a material that fulfills these conditions is found, alternatively, one could look for special cases in which odd-frequency pairing could be possible [17–19]. As pointed out by Matsumoto *et al.* [18], a plausible situation arises when an even frequency s-wave spin singlet (ESS) superconductor is placed in an external magnetic field, since the breaking of time-reversal symmetry is then expected to induce an OST component. However, despite this model proposal, the existence of time-odd superconductivity in real materials could thus far not be proven on the basis of a fully microscopic *ab initio* theory.

In this work, we report *ab initio* predictions of magnetic-field induced odd-frequency superconductivity in the two-band superconductor MgB_2. We develop the anisotropic Eliashberg framework of superconductivity with the inclusion of an external magnetic field, which allows for computing both time-even and time-odd superconductivity as self-consistent solutions. Taking as input the *ab initio* calculated electron and phonon band structure, as well as the momentum and frequency-resolved electron-phonon coupling, we solve self-consistently the Eliashberg equations for varying temperature and magnetic field values. Our calculations unambiguously show the existence of field-induced two-band OST superconductivity in MgB_2.

II. METHODOLOGY

To treat superconductivity in a magnetic field, we start from the microscopic Hamiltonian describing electrons, phonons, the electron-phonon interaction [20], and include the magnetic field as Zeeman interaction (see Appendix A). The matrix self-energy $\hat{\Sigma}(\mathbf{k},\omega_n)$, depending on momentum $\mathbf{k}$ and Matsubara frequency ω_n, contains the electron-phonon mass renormalization term, a term that renormalizes the magnetic field, and an even- and an odd-frequency gap function, $\Delta_{e(o)}(\mathbf{k},\omega_n)$. A diagrammatic expansion in the Migdal limit leads to four coupled equations for these four quantities, which are solved self-consistently in reciprocal space with *ab initio* input (see Appendices A and B).

The two-band superconductor MgB_2 ($T_c = 39$ K) [21,22] is an ideal candidate to study magnetic field induced OST superconductivity. MgB_2 is described thoroughly by *ab initio* methods [23]. Its Fermi surface consists of sheets with primarily π or σ orbital character [24]. High frequency in-plane boron modes lead to an enhanced, very anisotropic electron-phonon coupling that mediates the pairing [25,26]. Near the center of the Brillouin zone, the electron-phonon coupling well exceeds $\lambda_{\mathbf{q}} \approx 2$ [26]. Thus, for some regions in momentum space, the electron-phonon interaction in MgB_2 becomes strongly coupled and moderately retarded, therefore the possibility for odd-frequency pairing is enhanced. Due to the inherent anisotropy, superconductivity in MgB_2 is characterized by a

*alex.aperis@physics.uu.se

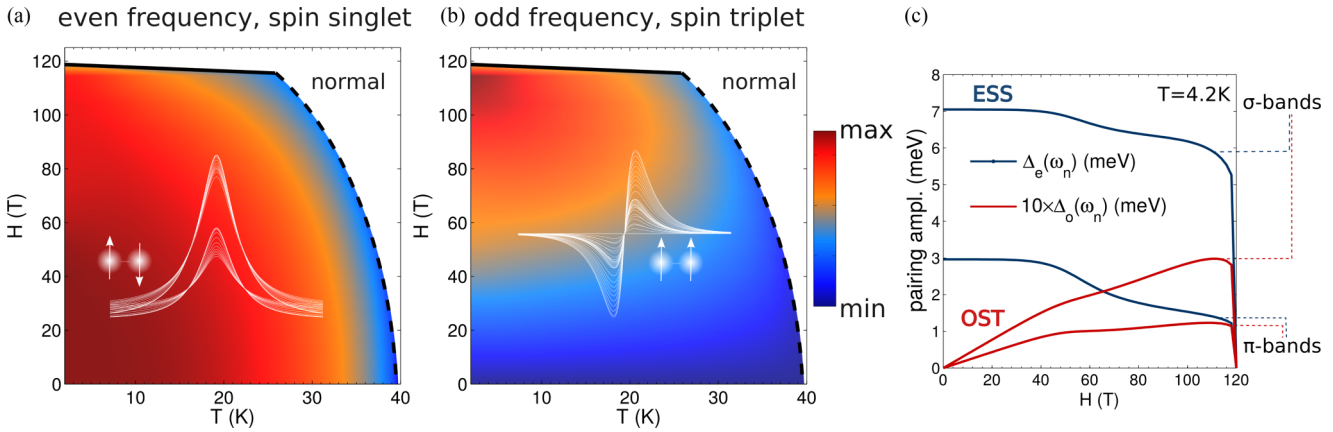

FIG. 1. (Color online) *Ab initio* computed temperature and magnetic field dependence of superconductivity in MgB_2. (a) H-T phase diagram of the even-frequency superconducting component. Dashed (solid) lines denote second (first) order transitions. (b) H-T phase diagram for the odd-frequency superconductivity. The insets show the Matsubara frequency dependence of each component for several magnetic field values. The two-gap structure, characteristic of superconductivity in MgB_2, can also be discerned. The colorbar value "max" ("min") corresponds to 7 meV (0 meV) and 0.3 meV (0 meV) for even- and odd-frequency superconductivity, respectively. (c) Band-resolved magnetic field dependence of the even and odd pairing amplitudes at low temperature. The lines correspond to the maximum values in Matsubara space of the momentum averaged superconducting pairing fields on each band, i.e., the peaks of the insets in (a) and (b). Note that the OST pairing amplitude is an order of magnitude smaller than the respective ESS one.

very anisotropic s-wave, two-gap structure ($\Delta_\pi = 2.8$ meV and $\Delta_\sigma = 7$ meV) [27], which can be explained with unprecedented precision by the fully anisotropic Eliashberg theory [28,29]. Our *ab initio* results for zero field completely confirm the previous calculations, which supports the accuracy of our self-consistent solutions for finite magnetic fields (see Appendix C).

III. RESULTS

In Fig. 1, we show the calculated magnetic field–temperature phase diagram for the ESS and OST superconducting components. For $H > 0$, the OST superconductivity appears and coexists with the ESS component in the same H-T regime where the latter is nonzero. The H-T dependence of the ESS superconductivity follows that of a Pauli limited superconductor; it goes to zero monotonously via a second-order phase transition with temperature, except for a very narrow region near the upper critical field (H_p), where the transition becomes first order. The transition to the normal state with the field changes from first to second order above $T \approx 26$ K. Our solutions provide the first *ab initio* prediction for the paramagnetic limiting field of MgB_2 (see, e.g., Ref. [30]), when orbital effects are neglected. We find $H_p = 119$ T, which is significantly less than previous estimations (140 T) [31]. Notably, MgB_2 is a type II superconductor in which a vortex state yields an orbitally limited upper-critical field. However, as has been shown for MgB_2 thin films, the upper critical field can be greatly enhanced towards the Pauli limit when the field is applied in-plane and may well reach $H_{c_2} \approx 70$ T [32]. Also, new thin films with greatly enhanced lower critical fields ($H_{c_1} > 40$ T) have recently become available [33]. For such films, the calculated phase diagrams in Fig. 1 should be valid up to 40 T. Since the here-computed odd-frequency superconductivity depends only on the applied field, it should be finite in the vortex state, as well. At low temperatures, the two ESS superconducting gaps remain almost constant up to $H_\pi \approx 39$ T, as shown in Fig. 1(c). This is the lowest field strength needed to overcome the binding energy of the Cooper pairs originating from the π band. Increasing the field further, leads to partial destruction of the latter gap and the concomitant decrease of the σ gap, due to the strong interband electron-phonon coupling in MgB_2.

The OST component behaves similar to the ESS as concerns the order of the transitions to the normal state and its temperature evolution. However, it exhibits a distinctively different magnetic field dependence; it follows a re-entrant behavior with the field, as is shown in Fig. 1(b). The trend becomes clearer at higher temperature where the re-entrance peak moves away from H_p. From Fig. 1(c), one can observe that there exists, up to $H \approx 39$ T, a linear dependence of OST state on the magnetic field irrespective of the band index. Notably, the OST superconductivity also has a two-gap structure but the pairing is much weaker than the respective ESS component. In the absence of the magnetic field, the OST component is zero.

Next, we examine the Fermi surface momentum dependence of the superconducting gaps, presented in Fig. 2. In the Eliashberg framework, the gap is frequency dependent and in general complex [cf. Figs. 2(c) and 2(f)]. Its real part $\Delta'_{e(o)}(\mathbf{k},\omega)$ for the ESS (OST) superconductivity is related to the measurable gap edge, whereas the imaginary part $\Delta''_{e(o)}(\mathbf{k},\omega)$ corresponds to the damping of quasiparticle excitations by decay with phonon emission. The gap edge in the *anisotropic*, zero-field case is given by $\Delta'(\mathbf{k},\omega_\mathbf{k}) = \omega_\mathbf{k}$ [28]. However, here the applied magnetic field lifts the degeneracy between spin $\sigma = \uparrow,\downarrow$ quasiparticles, providing the Zeeman splitting. As a consequence, external probes see a superconducting gap edge that is effectively split in two. Moreover, the presence of the OST superconductivity further modifies the gap edge. The relevant expressions can be found from the poles in the system's Green's functions at the Fermi level,

$$\omega_{\mathbf{k},\sigma} = -\sigma\tilde{H}'(\mathbf{k},\omega_{\mathbf{k},\sigma}) + \Delta'_e(\mathbf{k},\omega_{\mathbf{k},\sigma}) + \sigma\,\Delta'_o(\mathbf{k},\omega_{\mathbf{k},\sigma}), \quad (1)$$

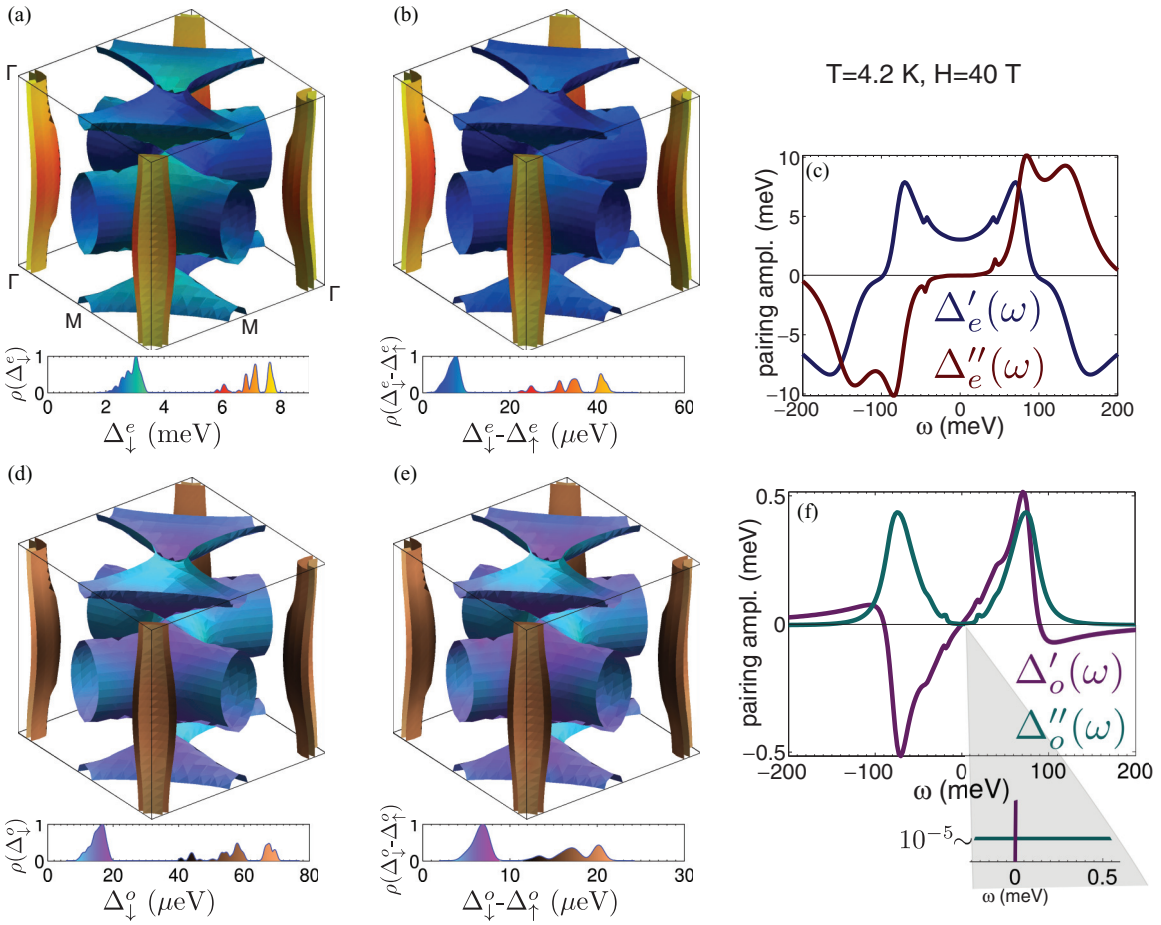

FIG. 2. (Color online) Computed momentum and frequency dependence of superconductivity in MgB_2 at $T = 4.2$ K and $H = 40$ T. (a) The Fermi surface of MgB_2 in the conventional Brillouin zone colored by the values of the even-frequency superconducting gap edge $\Delta^e_\downarrow(\mathbf{k})$ for spin-↓ quasiparticles. The distribution of the gap edge values is shown in the inset below. (b) The difference between spin-↓ and spin-↑ even-frequency superconducting gap edges. (c) Typical frequency dependence of the real $[\Delta'_e(\mathbf{k}_0,\omega) \equiv \Delta'_e(\omega)]$ and imaginary $[\Delta''_e(\mathbf{k}_0,\omega) \equiv \Delta''_e(\omega)]$ part of the ESS pairing amplitude at a given point $\mathbf{k}_0$ on the Fermi surface. (d) and (e) Same as in (a) and (b), but for the odd-frequency superconducting gap edge. (f) Same as in (c), but for the real $[\Delta'_o(\omega)]$ and imaginary $[\Delta''_o(\omega)]$ parts of the OST pairing amplitude. Near $\omega = 0$, $\Delta'_o(\omega)$ increases linearly with frequency, whereas $\Delta''_o(\omega)$ is almost constant. The latter is finite at $\omega = 0$ as shown in the inset.

where $\tilde{H}'(\mathbf{k},\omega_\mathbf{k})$ is the renormalized magnetic field term that includes self-energy contributions (see Appendix A). In the above, the OST spins are perpendicular to H. We define an effective $\mathbf{k}$-dependent gap edge as $\Delta^{e(o)}_{\uparrow(\downarrow)}(\mathbf{k}) = \Delta'_{e(o)}(\mathbf{k},\omega_{\mathbf{k},\uparrow(\downarrow)})$. The distribution of gap edge values is denoted as $\Delta^{e(o)}_{\uparrow(\downarrow)}$ (see insets of Fig. 2).

Since the real part of the OST order parameter $\Delta_o(\mathbf{k},\omega_\mathbf{k})$ vanishes at $\omega = 0$ [see Fig. 2(f)], the gap edge of a pure odd-frequency superconductor should be zero. However, due to the presence of the ESS superconductivity and the magnetic field, this is finite in our case. In Fig. 2(a), we show the full momentum dependence of the spin-↓ ESS gap edge over the Fermi surface of MgB_2. The 3D tubular networks are due to the π bands, while the almost two-dimensional cylinders are due to the σ bands [24]. The two-gap structure is similar to the zero-field case [28] but the momentum anisotropy differs. For the π bands, we find gap values between 1.8–3.5 meV, which are close to the zero-field values, while for the σ bands, we find gap values between 5.6–8 meV and thus an enhanced anisotropy. Figure 2(b) shows the difference between the spin-split gap edges of the ESS component. Remarkably, the splitting is more efficient for the σ bands where the gap edge is larger.

As shown in Fig. 2(d), the OST gap edge is very anisotropic and at $H = 40$ T it is two orders of magnitude smaller than the respective ESS component. Comparing Figs. 2(d) and 2(b), we find that $\Delta^o_\downarrow(\mathbf{k})$ is proportional to the difference of the ESS gap edges for the two spin components. This finding directly evidences that the OST superfluid density is proportional to the number density of spin flipped carriers that participate in the ESS Cooper pairs. Therefore the OST is subordinate to the ESS state.

IV. PREDICTIONS FOR EXPERIMENTAL DETECTION

From the spectral function of our system, we have derived the quasiparticle density of states (DOS) in the superconducting state, $N(\omega) = \sum_\sigma N_\sigma(\omega)$. This quantity is proportional to the differential conductance measured in tunneling experiments [29]. Here, we study a normal metal/insulator/MgB_2 junction. An experimental setup with an in-plane field and

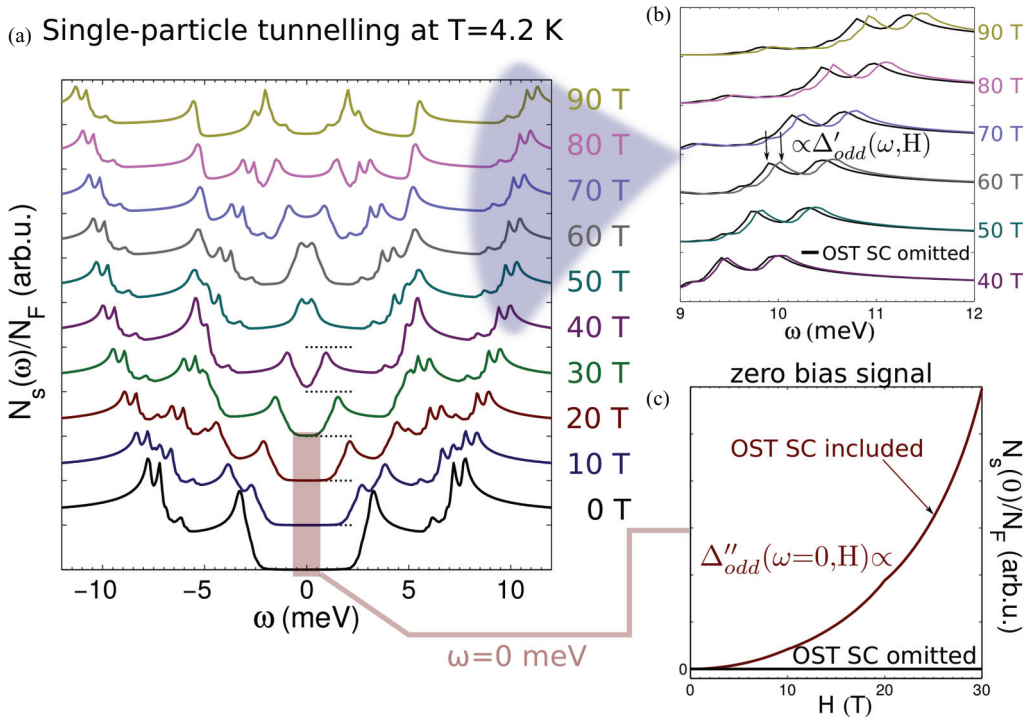

FIG. 3. (Color online) Predicted dependence of single-particle tunneling spectra on the magnetic field. (a) Low-temperature superconducting density of states of MgB_2 for several values of the external magnetic field. (b) Comparison between tunneling spectra when the odd-frequency pairing is included in the Eliashberg calculation and when it is not (black lines). As the field increases, the odd-frequency gap induces a shift in the tunneling peaks of the order of 0.1 meV. This shift is pronounced for the superconducting gap over the σ bands. (c) In the absence of external bias, we predict a nonzero signal in the tunneling spectra that is proportional to the imaginary part of the OST gap. This has a distinct magnetic field dependence, the detection of which will serve as a definite proof for the existence of odd-frequency superconductivity in MgB_2.

carriers injected along the field would minimize the orbital effects and would therefore best compare with our reported results. The spin-resolved quasiparticle DOS reads

$$\frac{N_\sigma(\omega)}{N_F} = \frac{1}{2}\mathrm{Re}\langle|\omega+\sigma\tilde{\mathrm{H}}(\mathbf{k},\omega)|[(\omega+\sigma\tilde{\mathrm{H}}(\mathbf{k},\omega))^2 - (\Delta_e(\mathbf{k},\omega)+\sigma\Delta_o(\mathbf{k},\omega))^2]^{-\frac{1}{2}}\rangle_{\mathbf{k}}, \quad (2)$$

where N_F is the DOS at the Fermi level in the normal state and $\langle\ldots\rangle_{\mathbf{k}}$ denotes Fermi surface averaging. Using our self-consistent data in Eq. (2), we calculate the magnetic field evolution of the tunneling spectra at low temperature, shown in Fig. 3(a). For $H=0$, we find two peaks around 3 and 7 meV that signal the quasiparticle excitations above the π and the σ gaps, respectively [28,29]. We also obtain the recently observed fine momentum structure of the latter gap [29]. As the field increases, the peaks begin to split due to the spin degeneracy lifting. This is clearly visible already at 10 T for the π peak, while at 20 T, the splitting in both peaks should be very clearly resolved. The gap starts to close around 39 T where the magnetic field strength is comparable to the minimum gap edge value on the π bands.

The odd-frequency component is finite for finite field and increases linearly with ω in the low frequency regime [cf. Fig. 2(f)]. Thus one would generally expect the OST gap to manifest as a shift of the tunneling peaks for finite ω, to higher (lower) ω due to destructive (constructive) interference with the dominant ESS gap. However, due to the smallness of the OST gap, these effects are practically washed out by the dominant ESS component except for two regions. The first one is for fields near 39 T, just before the π gap begins to close. There, the OST gap reduces the magnetic field threshold of the zero energy peak by 0.5 T. The second is at frequencies near the σ-band peak, where the OST component shifts the peak to the right. For 40 T, the calculated peak shift is around 100 μeV and increases with the field as seen in Fig. 3(b).

We now focus on the zero bias regime, $\omega=0$. This case is of special interest, since all lifetime effects coming from the electron-phonon and the Zeeman interaction are absent. The real part of the induced OST gap is also zero [Fig. 2(f)] but the situation differs from that in a pure OST superconductor since here the ESS component provides a robust gap at the Fermi level. Hence no low-lying excitations should be expected at low temperatures and small, comparing to the π gap, magnetic fields. This is certainly true for $H=0$ [Fig. 2(a)]. However, when the field is turned on, the imaginary part of the OST component $\Delta_o''(\mathbf{k},0)$ becomes finite [Fig. 2(f)]. This term stems from damping processes of the quasiparticle excitations caused by the magnetic field. It contributes an additional lifetime broadening to the quasiparticles and remarkably enforces a nonzero result in Eq. (2) even at $\omega=0$. If the OST is not included in the theory, the latter is ideally zero. Therefore a zero-bias signal in the single-particle tunneling appears due to the induced OST superconducting component. The predicted signal has a distinct magnetic field dependence, as is shown in Fig. 3(c), which stands out from any zero-bias noise signal. The

same should hold even in the presence of vortices, since these contribute a completely different field dependence [34,35]. This zero-bias plateau is even more pronounced for $T < 4.2$ K where the OST state is more favored [Fig. 1(b)]. Thus we propose that a measurement of the zero-bias tunneling under magnetic fields less than ∼39 T and at low temperatures would serve as definite proof for the identification of odd-frequency superconductivity in MgB_2 and in any superconductor that supports this kind of state.

V. CONCLUSIONS

Our precise quantitative *ab initio* calculations predict the existence of odd-frequency superconductivity in MgB_2, provide an in-depth insight into the microscopic nature of this exotic state, and pave the way for its ultimate experimental detection. Furthermore, our approach initiates a novel *ab initio* "roadmap" for the search of exotic magnetic-field-induced phenomena (for example, Refs. [36,37]) relevant for both bulk and interface physics [10,12,38].

ACKNOWLEDGMENTS

We thank G. Varelogiannis for fruitful discussions. This work has been supported by the Swedish Research Council (VR) and the Swedish National Infrastructure for Computing (SNIC).

APPENDIX A: ELIASHBERG THEORY FOR FIELD-INDUCED ODD-FREQUENCY SUPERCONDUCTIVITY

We start with the most general microscopic Hamiltonian describing electrons, phonons, and electron-phonon and Zeeman interactions in a metal,

$$\begin{aligned} H = &\sum_{\mathbf{k}} \xi_{\mathbf{k}} \Psi^{\dagger}_{\mathbf{k}} \hat{\rho}_3 \hat{\sigma}_0 \Psi_{\mathbf{k}} + \sum_{\mathbf{q},\nu} \hbar\omega_{\mathbf{q}\nu} \left(b^{\dagger}_{\mathbf{q}\nu} b_{\mathbf{q}\nu} + \frac{1}{2} \right) \\ &+ \sum_{\mathbf{q},\nu} \sum_{\mathbf{k},\mathbf{k}'} g^{\nu}_{\mathbf{q}} u_{\mathbf{q}\nu} \Psi^{\dagger}_{\mathbf{k}'} \hat{\rho}_3 \hat{\sigma}_0 \Psi_{\mathbf{k}} \\ &+ \frac{1}{2} \sum_{\mathbf{k},\mathbf{k}',\mathbf{q}} \Psi^{\dagger}_{\mathbf{k}'} \hat{\rho}_3 \hat{\sigma}_0 \Psi_{\mathbf{k}'} V_{\mathbf{k}'-\mathbf{k}} \Psi^{\dagger}_{\mathbf{k}} \hat{\rho}_3 \hat{\sigma}_0 \Psi_{\mathbf{k}} \\ &+ \mu_B h \sum_{\mathbf{k}} \Psi^{\dagger}_{\mathbf{k}} \hat{\rho}_3 \hat{\sigma}_3 \Psi_{\mathbf{k}}, \end{aligned} \tag{A1}$$

compactly written using the following spinor:

$$\Psi^{\dagger}_{\mathbf{k}} = \frac{1}{\sqrt{2}} (c^{\dagger}_{\mathbf{k}\uparrow}, c^{\dagger}_{\mathbf{k}\downarrow}, c_{-\mathbf{k}\uparrow}, c_{-\mathbf{k}\downarrow}) \tag{A2}$$

acting on the Pauli basis spanned by $\hat{\rho}_i \otimes \hat{\sigma}_j$, with $i,j = 0,1,2,3$. In the above, $\xi_{\mathbf{k}}$ is the electron dispersion, which in our case is calculated *ab initio* and h is an external magnetic field, $\omega_{\mathbf{q}\nu}$, $g^{\nu}_{\mathbf{q}}$ are the branch-resolved phonon frequencies and electron-phonon coupling matrix elements, also calculated *ab initio*. As usual, the second quantized displacement operator for the phonons is denoted as $u_{\mathbf{q}\nu}$, and $c_{\mathbf{k}}$ ($c^{\dagger}_{\mathbf{k}}$) are electron and $b_{\mathbf{q}\nu}$ ($b^{\dagger}_{\mathbf{q}\nu}$) phonon annihilation (creation) operators, respectively.

The full matrix Green's function follows from the Dyson equation

$$\hat{G}(\mathbf{k},n) = \left[\hat{G}^{-1}_0(\mathbf{k},n) - \hat{\Sigma}(\mathbf{k},n) \right]^{-1}, \tag{A3}$$

with the free matrix propagator

$$\hat{G}_0(\mathbf{k},n) = (i\omega_n \hat{\rho}_0 \hat{\sigma}_0 - \xi_{\mathbf{k}} \hat{\rho}_3 \hat{\sigma}_0 - \mu_B h \hat{\rho}_3 \hat{\sigma}_3)^{-1}, \tag{A4}$$

where $\omega_n = (2n+1)\pi k_B T$ are fermionic Matsubara frequencies. The self-energy is calculated by a diagrammatic expansion in the Migdal limit:

$$\hat{\Sigma}(\mathbf{k},n) = T \sum_{\mathbf{k}',n'} \frac{1}{N_F} [\lambda(\mathbf{k},\mathbf{k}';n,n) - \mu^*] \hat{\rho}_3 \hat{\sigma}_0 \hat{G}(\mathbf{k}',n') \hat{\rho}_3 \hat{\sigma}_0, \tag{A5}$$

where the momentum-dependent electron-phonon coupling is

$$\lambda(\mathbf{k},\mathbf{k}';n,n') = \int_0^{\infty} d\Omega \alpha^2 F(\mathbf{k},\mathbf{k}';\Omega) \frac{2\Omega}{(\omega_n - \omega_{n'})^2 + \Omega^2}, \tag{A6}$$

with the momentum-dependent Eliashberg function

$$\alpha^2 F(\mathbf{k},\mathbf{k}';\Omega) = N_F \sum_{\nu} \left| g^{\nu}_{\mathbf{k},\mathbf{k}'} \right|^2 \delta(\Omega - \omega_{\mathbf{k},\mathbf{k}'\nu}). \tag{A7}$$

Both quantities in (A6) and (A7) were calculated *ab initio* using density functional perturbation theory. With N_F we denote the DOS at the Fermi level and μ^* is the Anderson-Morel Coulomb pseudopotential.

The matrix self-energy in our studied case has the form

$$\begin{aligned} \hat{\Sigma}(\mathbf{k},n) = &(1 - Z(\mathbf{k},n)) i\omega_n \hat{\rho}_0 \hat{\sigma}_0 + \chi(\mathbf{k},n) \hat{\rho}_3 \hat{\sigma}_0 \\ &+ \Sigma_h(\mathbf{k},n) \hat{\rho}_3 \hat{\sigma}_3 + \phi_e(\mathbf{k},n) \hat{\rho}_2 \hat{\sigma}_2 + i\phi_o(\mathbf{k},n) \hat{\rho}_1 \hat{\sigma}_1. \end{aligned} \tag{A8}$$

Here, $Z(\mathbf{k},n)$ is the mass renormalization function, $\Sigma_h(\mathbf{k},n)$ is the self-energy that renormalizes the magnetic field and $\phi_e(\mathbf{k},n)$, $i\phi_o(\mathbf{k},n)$ describe anisotropic s-wave even-frequency spin singlet and odd-frequency spin triplet superconducting pairing, respectively [18]. In what follows, we omit the electron dispersion self-energy, $\chi(\mathbf{k},n)$, since this cancels out when we integrate over energy. We have taken the magnetic field and the **d** vector of the odd-frequency spin triplet superconductivity to lie along the z axis. We note that in our calculations the effect of the external magnetic field is included as a first-order perturbation of the electronic energy dispersions calculated *ab initio* at zero field. In this sense, the external magnetic field is not included self-consistently, but since the Zeeman splittings are, even for fields of up to 100 T, only of the order of a few meVs, the non-self-consistency is not expected to play any role.

After integrating over energy, we are left with the following system of four coupled self-consistent Eliashberg equations that depend on momentum and Matsubara frequency:

$$Z(\mathbf{k},n) = 1 + \frac{1}{2\omega_n} \pi T \sum_{n',\pm} \left\langle \lambda(\mathbf{k},\mathbf{k}';n,n') \frac{\omega_{n'} \pm i\tilde{\mathrm{H}}(\mathbf{k}',n')}{D(\mathbf{k}',n')} \right\rangle_{\mathbf{k}'}, \tag{A9}$$

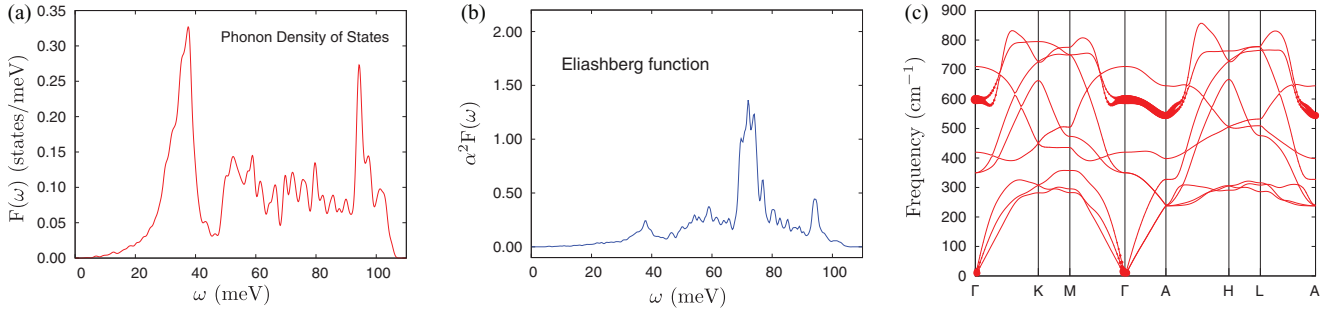

FIG. 4. (Color online) *Ab initio* calculated electron-phonon properties of MgB_2. (a) Computed phonon density of states. (b) Momentum-integrated Eliashberg function. (c) Phonon dispersion relations along high-symmetry lines. The radius of the symbols is proportional to the strength of the electron-phonon coupling for each phonon mode, $\lambda_{\mathbf{q}\nu}$.

$$\Sigma_h(\mathbf{k},n) = \frac{1}{2}\pi T \sum_{n',\pm}\left\langle \lambda(\mathbf{k},\mathbf{k}';n,n')\frac{\tilde{\mathrm{H}}(\mathbf{k}',n') \mp i\omega_{n'}}{D(\mathbf{k}',n')}\right\rangle_{\mathbf{k}'}, \tag{A10}$$

$$Z(\mathbf{k},n)\Delta_e(\mathbf{k},n) = \frac{1}{2}\pi T \sum_{n',\pm}\left\langle [\lambda(\mathbf{k},\mathbf{k}';n,n') - \mu^*] \times \frac{\Delta_e(\mathbf{k}',n') \mp i\Delta_o(\mathbf{k}',n')}{D(\mathbf{k}',n')}\right\rangle_{\mathbf{k}'}, \tag{A11}$$

$$Z(\mathbf{k},n)\Delta_o(\mathbf{k},n) = \frac{1}{2}\pi T \sum_{n',\pm}\left\langle [\lambda(\mathbf{k},\mathbf{k}';n,n') - \mu^*] \times \frac{\Delta_o(\mathbf{k}',n') \pm i\Delta_e(\mathbf{k}',n')}{D(\mathbf{k}',n')}\right\rangle_{\mathbf{k}'}, \tag{A12}$$

with

$$D(\mathbf{k}',n') = [(\omega_{n'} \pm i\tilde{\mathrm{H}}(\mathbf{k}',n'))^2 + (-\Delta_e(\mathbf{k}',n') \pm i\Delta_o(\mathbf{k}',n'))^2]^{\frac{1}{2}}. \tag{A13}$$

In the above, $\langle\cdots\rangle_{\mathbf{k}} = \sum_{\mathbf{k}} \frac{\delta(\xi_{\mathbf{k}})}{N_F}$ denotes a Fermi surface average, $\mathrm{H}(\mathbf{k}',n') = \Sigma_h(\mathbf{k}',n') + \mu_B h$, and $\tilde{\mathrm{H}}(\mathbf{k}',n') = \mathrm{H}(\mathbf{k}',n')/Z(\mathbf{k}',n')$.

The quasiparticle density of states that is proportional to single-particle tunneling measurements, is

$$N_s(\omega) \propto \sum_{\mathbf{k}} A(\mathbf{k},\omega) \approx N_F\left\langle \int_{-\infty}^{\infty} d\xi\, A_{\mathbf{k}}(\xi,\omega)\right\rangle_{\mathbf{k}_F} \tag{A14}$$

with the spectral function

$$A(\mathbf{k},\omega) = -\frac{1}{4\pi}\mathrm{ImTr}[\hat{G}_R(\mathbf{k},\omega)], \tag{A15}$$

where $\hat{G}_R(\mathbf{k},\omega)$ is the retarded Green's function obtained after analytic continuation of Eq. (A3).

APPENDIX B: PHONON AND ELECTRON-PHONON COUPLING CALCULATIONS

The ground-state properties of MgB_2 are calculated using density functional theory (DFT) in the local-density approximation (LDA) as implemented in the code ABINIT [39]. The electron-ionic core interaction on the valence electrons in the systems has been represented by the projector-augmented wave potentials (PAW) [40], and the wave functions are expanded in plane waves with an energy cutoff at 24 Hartree and a cutoff for the double grid of 32 Hartree.

The calculated lattice parameters for the MgB_2 hexagonal structure ($P6/mmm$) are $a = 3.038$ Å and $c = 3.462$ Å. The electron-phonon coupling is computed as response function within the density-functional perturbation theory. We use a $24 \times 24 \times 24$ k-point grid in the Brillouin zone for the self-consistent calculations and a $12 \times 12 \times 6$ grid for the Fermi surface properties. Our results for the phonon DOS, the Eliashberg function, and the phonon frequency dispersions are shown in Fig. 4.

APPENDIX C: NUMERICAL SOLUTION OF THE ELIASHBERG EQUATIONS

The coupled equations (A9)–(A12), supplemented by the electron and phonon band structure and the electron-phonon coupling, calculated by first principles, were solved self-consistently in Matsubara space and the converged solutions were then analytically continued to real frequencies. In

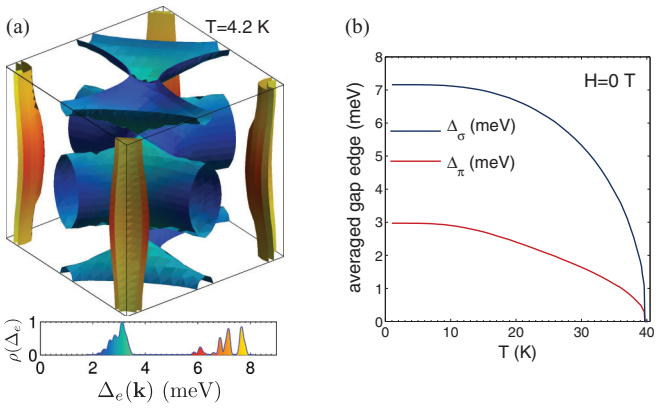

FIG. 5. (Color online) Calculated momentum and temperature dependence of superconductivity in MgB_2 at zero field. (a) The Fermi surface of MgB_2 in the conventional Brillouin zone colored by the values of the even-frequency superconducting gap edge [$\mathrm{Re}\,\Delta_{\mathbf{k}}(\omega) = \omega$] at $T = 4.2$ K and $H = 0$ T. The distribution of the gap edge values is shown in the inset below. (b) Temperature dependence of the even-frequency superconducting gap edges, momentum-averaged over the σ and π Fermi surface sheets.

order to ensure a good accuracy for both the ESS and the OST gaps, we imposed a strict convergence criterion of $\frac{x_n - x_{n-1}}{x_n} < 10^{-8}$ and allowed up to 4000 iteration cycles. In all the calculations presented here, we set $\mu^*(\omega_c) = 0.16$ for the Coulomb pseudopotential with a cut-off frequency $\omega_c = 0.5$ eV. With these parameters we obtain $T_c = 39.8$ K for $H = 0$.

For completeness, we mention that the same calculations with $\mu^*(\omega_c) = 0.165$ give $T_c = 39.1$ K. We have also checked that ω_c is sufficiently large and that results do not change by increasing this cutoff. The analytic continuation was performed numerically by employing the high-accuracy Padé scheme based on symbolic computation of Beach, Gooding, and Marsiglio [41] with a chosen precision of 250 decimal digits.

Our results for zero magnetic field are in excellent agreement with experiments and the theory reported previously [28], as can be seen in Fig. 5. For completeness, we also report here the frequency dependence of the analytically continued superconducting pair amplitude (Fig. 6), which is also in good agreement with previous work [42].

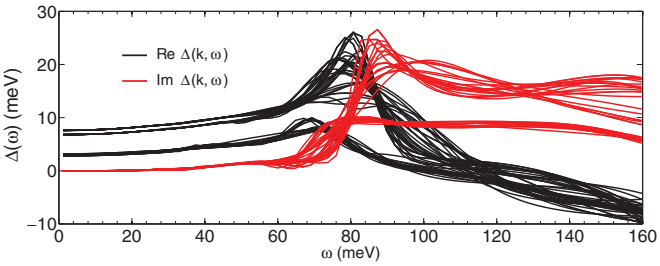

FIG. 6. (Color online) Calculated frequency dependence of superconductivity in MgB_2 at $T = 4.2$ K and zero field. Real (black) and imaginary (red) parts of the even-frequency superconducting pair amplitude $\Delta(\mathbf{k},\omega)$ at several Fermi surface points.

[1] M. Sigrist and K. Ueda, Rev. Mod. Phys. **63**, 239 (1991).
[2] V. L. Berezinskii, JETP Lett. **20**, 287 (1974).
[3] T. R. Kirkpatrick and D. Belitz, Phys. Rev. Lett. **66**, 1533 (1991).
[4] A. Balatsky and E. Abrahams, Phys. Rev. B **45**, 13125 (1992).
[5] P. Coleman, E. Miranda, and A. Tsvelik, Phys. Rev. B **49**, 8955 (1994).
[6] I. I. Mazin and M. D. Johannes, Nat. Phys. **1**, 91 (2005).
[7] F. S. Bergeret, A. F. Volkov, and K. B. Efetov, Rev. Mod. Phys. **77**, 1321 (2005).
[8] Y. Tanaka and A. A. Golubov, Phys. Rev. Lett. **98**, 037003 (2007).
[9] M. Eschrig and T. Löfwander, Nat. Phys. **4**, 138 (2008).
[10] Y. Tanaka, M. Sato, and N. Nagaosa, J. Phys. Soc. Jpn. **81**, 011013 (2012).
[11] Y. Asano, Y. V. Fominov, and Y. Tanaka, Phys. Rev. B **90**, 094512 (2014).
[12] H. Ebisu, K. Yada, H. Kasai, and Y. Tanaka, Phys. Rev. B **91**, 054518 (2015).
[13] *100 Years of Superconductivity*, edited by H. Rochalla and P. H. Kes (CRC Press, Bocca Raton, USA, 2011).
[14] D. Solenov, I. Martin, and D. Mozyrsky, Phys. Rev. B **79**, 132502 (2009).
[15] H. Kusunose, Y. Fuseya, and K. Miyake, J. Phys. Soc. Jpn. **80**, 054702 (2011).
[16] H. Kusunose, Y. Fuseya, and K. Miyake, J. Phys. Soc. Jpn. **80**, 044711 (2011).
[17] Y. Fuseya, H. Kohno, and K. Miyake, J. Phys. Soc. Jpn. **72**, 2914 (2003).
[18] M. Matsumoto, M. Koga, and H. Kusunose, J. Phys. Soc. Jpn. **81**, 033702 (2012).
[19] A. M. Black-Schaffer and A. V. Balatsky, Phys. Rev. B **88**, 104514 (2013).
[20] F. Marsiglio and J. P. Carbotte, in *Superconductivity*, edited by K. H. Bennemann and J. B. Ketterson (Springer, Berlin, 2008), pp. 73–162.
[21] J. Nagamatsu, N. Nakagawa, T. Muranaka, Y. Zenitani, and J. Akimitsu, Nature (London) **410**, 63 (2001).
[22] S. Souma, Y. Machida, T. Sato, T. Takahashi, H. Matsui, S.-C. Wang, H. Ding, A. Kaminski, J. C. Campuzano, S. Sasaki, and K. Kadowaki, Nature (London) **423**, 65 (2003).
[23] J. M. An and W. E. Pickett, Phys. Rev. Lett. **86**, 4366 (2001).
[24] J. Kortus, I. I. Mazin, K. D. Belashchenko, V. P. Antropov, and L. L. Boyer, Phys. Rev. Lett. **86**, 4656 (2001).
[25] K.-P. Bohnen, R. Heid, and B. Renker, Phys. Rev. Lett. **86**, 5771 (2001).
[26] H. J. Choi, D. Roundy, H. Sun, M. L. Cohen, and S. G. Louie, Phys. Rev. B **66**, 020513 (2002).
[27] P. Szabó, P. Samuely, J. Kačmarčík, T. Klein, J. Marcus, D. Fruchart, S. Miraglia, C. Marcenat, and A. G. M. Jansen, Phys. Rev. Lett. **87**, 137005 (2001).
[28] H. J. Choi, D. Roundy, H. Sun, M. L. Cohen, and S. G. Louie, Nature (London) **418**, 758 (2002).
[29] K. Chen, W. Dai, C. Zhuang, Q. Li, S. Carabello, J. G. Lambert, J. T. Mlack, R. C. Ramos, and X. X. Xi, Nat. Commun. **3**, 619 (2012).
[30] C. B. Eom, M. K. Lee, J. H. Choi, L. J. Belenky, X. Song, L. D. Cooley, M. T. Naus, S. Patnaik, J. Jiang, M. Rikel, A. Polyanskii, A. Gurevich, X. Y. Cai, S. D. Bu, S. E. Babcock, E. E. Hellstrom, D. C. Larbalestier, N. Rogado, K. A. Regan, M. A. Hayward, T. He, J. S. Slusky, K. Inumaru, M. K. Haas, and R. J. Cava, Nature (London) **411**, 558 (2001).
[31] A. Gurevich, Physica C **456**, 160 (2007).
[32] V. Braccini, A. Gurevich, J. E. Giencke, M. C. Jewell, C. B. Eom, D. C. Larbalestier, A. Pogrebnyakov, Y. Cui, B. T. Liu, Y. F. Hu, J. M. Redwing, Q. Li, X. X. Xi, R. K. Singh, R. Gandikota, J. Kim, B. Wilkens, N. Newman, J. Rowell, B. Moeckly, V. Ferrando, C. Tarantini, D. Marré, M. Putti, C. Ferdeghini, R. Vaglio, and E. Haanappel, Phys. Rev. B **71**, 012504 (2005).
[33] D. B. Beringer, C. Clavero, T. Tan, X. X. Xi, W. M. Roach, and R. A. Lukaszew, IEEE Trans. Appl. Supercond. **23**, 7500604 (2013).
[34] M. R. Eskildsen, M. Kugler, S. Tanaka, J. Jun, S. M. Kazakov, J. Karpinski, and O. Fischer, Phys. Rev. Lett. **89**, 187003 (2002).

[35] Y. Bugoslavsky, Y. Miyoshi, G. K. Perkins, A. D. Caplin, L. F. Cohen, A. V. Pogrebnyakov, and X. X. Xi, Phys. Rev. B **72**, 224506 (2005).
[36] A. Aperis, M. Georgiou, G. Roumpos, S. Tsonis, G. Varelogiannis, and P. B. Littlewood, Europhys. Lett. **83**, 67008 (2008).
[37] A. Aperis, G. Varelogiannis, and P. B. Littlewood, Phys. Rev. Lett. **104**, 216403 (2010).
[38] J. Linder and J. W. A. Robinson, Nat. Phys. **11**, 307 (2015).
[39] X. Gonze *et al.*, Com. Phys. Comm. **180**, 2582 (2009).
[40] M. Torrent, F. Jollet, F. Bottin, G. Zérah, and X. Gonze, Comp. Mat. Sc. **42**, 337 (2008).
[41] K. S. D. Beach, R. J. Gooding, and F. Marsiglio, Phys. Rev. B **61**, 5147 (2000).
[42] E. R. Margine and F. Giustino, Phys. Rev. B **87**, 024505 (2013).